Hindawi
Complexity
Volume 2020, Article ID 1932406, 14 pages
https://doi.org/10.1155/2020/1932406

Research Article

Line Spectrum Chaotification on QZS Systems with Time-Delay Control

Jing Zhang, Tao Tang, and Wenhua Fang

School of Mechanical Engineering, Hunan Institute of Science and Technology, Yueyang 414006, China

Correspondence should be addressed to Jing Zhang; zhangjing819@hnu.edu.cn

Received 16 March 2020; Accepted 13 April 2020; Published 30 May 2020

Guest Editor: Shao-Bo He

Chaotification can be employed to weaken or eliminate the feature of line spectra of waterborne noise. The efficiency of this method lies on the use of small control. The analysis reveals that the critical control gain depends on the stiffness of vibration isolation systems. Thus, an isolation raft system based on quasi-zero-stiffness (QZS) property is proposed for line spectrum chaotification. A nonlinear time-delay controller is derived accordingly. Comparative analysis shows that the new approach allows much smaller control, and the intensity of line spectra is further reduced. Numerical simulations also indicate other advantages with the introduction of QZS system into chaotification.

1. Introduction

The spectra of the radiated waterborne noises of underwater vehicles are usually divided into two categories. One is continuous broadband spectra corresponding to noise induced by water current and bubble burst. The other is discrete narrowband line spectra mainly caused by propeller and machinery vibrations. Line spectra consist of closely spaced spectral lines that characterize the intensity of noise components. Line spectra of radiated noise from machinery vibration signify the features of operating underwater vehicles, such as the speed and distance of moving objects. Thus, line spectra have been generally utilized for identifying underwater vehicles and thus regarded as harmful signals for the vehicle safety.

Extensive efforts have been made to attenuate machinery vibrations for the reduction of noise spectra through vibration isolation techniques [1–3]. It has been known that the linear vibration isolation techniques can reduce the intensity of line spectra in a certain frequency bandwidth but cannot change the structure of line spectra of vibration noises due to the frequency fidelity. It means that a sinusoidal input of vibration source to an isolation system will simply turn out a sinusoidal output unable to eliminate the line spike at the frequency. To cope with the problem, an innovative idea [4] was proposed to change the spectra configuration by chaotification [4–7] rather than only rely on vibration attenuation. With a special mechanism, the response of the simple harmonic excitation from the vibration source to the base can present a chaotic state. The process can be called line spectrum chaotification, and the line spectrum structure without control and the line spectrum structure with control are shown in Figure 1. Chaotification is a new technique of making use of broadband nature of chaos to blur and change the feature of line spectra. The mechanism is that a nonlinear isolation system, installed in between the vibrating machine and supporting base, is designed with control which enables to convert a periodic excitation (narrowband input of machinery vibration) into a chaotic one (broadband output on a supporting base) to improve the concealment capability of underwater vehicles.

Lou et al. [4] first reported that a Duffing-type vibration isolator excited by harmonic forces might generate a broadband continuous spectrum at special parameter settings. Through a chaotification process, the intensity of line spectra transmitted to the base could be reduced. The feasibility of this approach was verified thoroughly in an experiment [5]. To enable chaotification for wider range of parameter settings, a parametric perturbation scheme [6] was proposed by using generalized chaos synchronization [8]. However, the

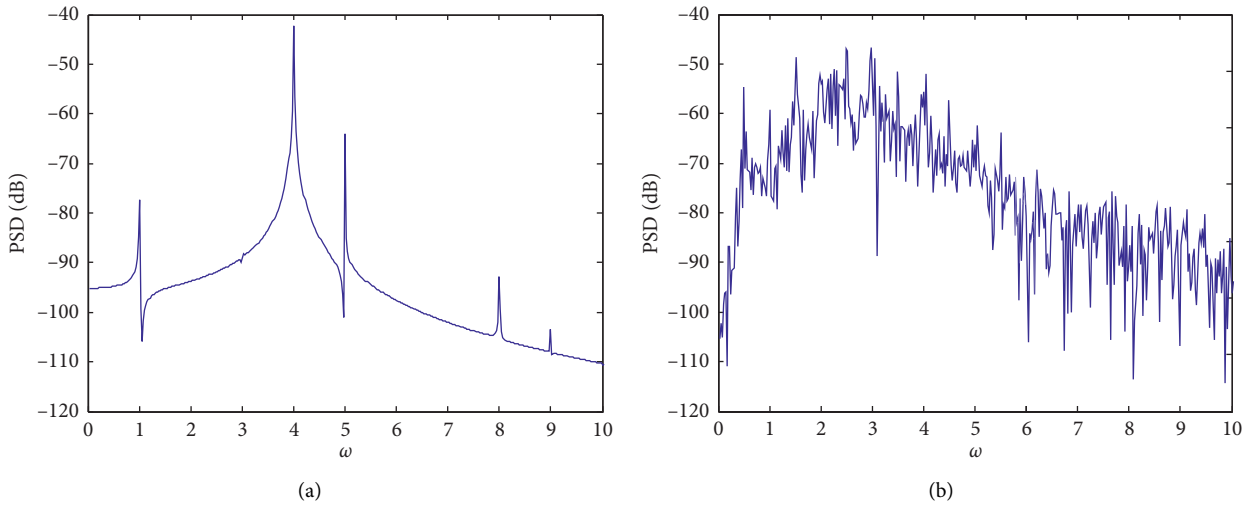

Figure 1: Comparison of line spectrum structure before (a) and after (b) chaotification.

persistence of chaotification may not be guaranteed since this scheme could deteriorate the system installation stability. This problem could be avoided by using a state perturbation approach [9]. Inspired by the work [8], chaotification [10] could be realized by employing the projective synchronization method [11], where a nonlinear vibration isolation system (VIS) is driven into a chaotic state by coupling a Duffing system. However, this approach requires large control energy and seems impractical for applications. We will elaborate later that control energy is very much concerned because not only there is a limitation of energy on board but also larger control energy may result in poor quality when reconstructing line spectra. A discrete impact method [12] based on Lyapunov exponents was proposed for chaotifying a Duffing type of VIS. This method also suffers the limitation for chaotification persistence and small controls.

It is known that the existence of time-delay feedback can extend a simple dynamic system into high dimensional one. This nature could make chaotification of a time-delay system readily applicable. In this regard, a new strategy by using time-delay feedback control was introduced for line spectrum chaotification [13–18]. Stability analysis [14] of a double-layer vibration isolation floating raft system (VIFRS) with a linear time-delay feedback control was carried out, and a set of critical criteria for stability switches are derived. These criteria provide a theoretical guidance for the setting of the system parameters and control parameters to achieve chaotification. Strictly speaking, these criteria are not necessary conditions but chaotification of VIFRS seems more likely with the criteria. For a better understanding, Li et al. [16] studied the dynamic behavior of the double-layer nonlinear isolation raft and revealed a variety of response solutions under time-delay control. Furthermore, chaotification of a two-dimensional VIFRS with dual time-delay feedback control was investigated [18]. A more sophisticated methodology originally developed from antichaos control [19, 20] could be employed for line spectrum reconstruction [17] of double-layer VIFRS. The significance of this work [17] is to provide a standard procedure for time-delay controller design which promises the occurrence of chaotification in the sense of Li and Yoke criteria [19]. This method based on nonlinear time-delay control notably outperforms the linear time-delay approaches [14, 18], especially in the requirement of small control. Different from the previous ideas, Zhou et al. [15] proposed a chaotification method totally based on spectrum optimization. This method can realize chaotification of VIFRS without exactly knowing system parameter settings or operational conditions, which is effective, easy to use, and handy in real applications.

The existing research works mainly focus on the generation of chaotic response in the floating raft isolation systems. In the purpose of altering the line spectrum configuration and eliminating spectrum line spikes, abundant results from numerical simulations [13, 15, 17] indicate that small control energy can lead to a better quality of chaotification in terms of the line spectrum intensity and broadness of spectrum bandwidth. Pursuing small control for chaotification is one of the key issues in the line spectrum reconfiguration. In this paper, we will propose time-delay control on a quasi-zero-stiffness (QZS) raft system for the improvement of both chaotification and isolation efficiency. The QZS system is a kind of nonlinear VIS with the characteristics of high static and low dynamic stiffness [21–25]. In the following study, we will first elaborate what factors affect the control energy. Then, we will introduce a newly developed QZS system [26] for line spectra control. Based on the new system, we will derive the nonlinear time-delay controller for chaotification. Numerical simulation will show the advance of the approach. By combining time-delay scheme with the QZS system, we can significantly decrease the critical control gain and meanwhile can effectively change the line spectrum configuration.

2. Critical Control Gain

In this section, we will state the key factors that dominate the minimum required control gain for chaotification, which is

referred to as critical control gain. Firstly, we look into a single degree-of-freedom (DOF) VIS and then extend the discussion to a double-layer VIS. Consider a nonlinear isolation system with a time-delay control:

$$\dot{x} = \mathbf{f}(\mathbf{x}) + \mathbf{g}(\mathbf{x})K_t\varphi(\tau_d), \tag{1}$$

where $\mathbf{x}$ is a state vector, $\mathbf{f}(\mathbf{x})$ and $\mathbf{g}(\mathbf{x}) \in R^n$ are vector field, K_t is a control gain, and $\varphi(\tau_d)$ is a time-delay feedback control function. The form of $\varphi(\tau_d)$ is not restricted which may be either linear or nonlinear function.

As shown in Figure 2(a), the mass m is supported by a nonlinear spring with quadratic and cubic nonlinearity, a linear damper, and an actuator which is utilized to implement time-delay feedback control. The governing equation of the single DOF mass-spring system with time-delay feedback control can be written as

$$\begin{aligned} &M\ddot{x} + C\dot{x} + K_1(x - \Delta x) + K_3(x - \Delta x)^3 \\ &\quad = F_0\cos(\omega_0 t) + K_t\varphi(\tau_d), \end{aligned} \tag{2}$$

where K_t is the feedback gain, $\varphi(\tau_d)$ is the time-delay feedback control function, C is the damping coefficient, K_1 and K_3 are the stiffness coefficients, F_0 and ω_0 are the amplitude and frequency of the harmonic excitation, respectively, and Δx denotes the static deformation of the spring subjected to the system static weight.

We define the following nondimensional parameters, and setting $X = x - \Delta x$,

$$\begin{aligned} \omega_n &= \sqrt{\frac{K_1}{M}}, \\ \xi &= \frac{C}{2M\omega_n}, \\ \eta &= \frac{K_3}{M}, \\ f_0 &= \frac{F_0}{M}, \\ \omega_t &= \sqrt{\frac{K_t}{M}}, \end{aligned} \tag{3}$$

the governing equation can be rewritten as

$$\ddot{X} + 2\xi\omega_n\dot{X} + \omega_n^2 X + \eta X^3 = f_0\cos\omega_0 t + \omega_t^2\varphi(\tau_d). \tag{4}$$

By defining $x_1 = X$ and $x_2 = \dot{X}$, the equation of motion without external excitation force can be written in the autonomous form:

$$\begin{cases} \dot{x}_1 = x_2, \\ \dot{x}_2 = -2\xi\omega_n x_2 - \omega_n^2 x_1 - \eta x_1^3 + \omega_t^2\varphi(\tau_d). \end{cases} \tag{5}$$

The system possess the equilibrium point $A(0,0)$. Giving a perturbed motion $(\Delta x_1, \Delta x_2)$ at the equilibrium point $A(0,0)$, it may yield two linearized time-delay differential equations:

$$\begin{cases} \Delta\dot{x}_1 = \Delta x_2, \\ \Delta\dot{x}_2 = -2\xi\omega_n\Delta x_2 - \omega_n^2\Delta x_1 + \omega_t^2\Delta x_1(t - \tau_d). \end{cases} \tag{6}$$

Note that the form of time-delay feedback control function $\varphi(\tau_d)$ may be arbitrary. If it is linear, the linearized part of $\varphi(\tau_d)$ is $\Delta x_1(t - \tau_d)$. If it is nonlinear, $\varphi(\tau_d)$ can be expressed in Taylor series of $\sum a_n\Delta x_1^n(t - \tau_d)$. Because of the vibration amplitude of a real VIS is often very small, the high order terms can be ignored and the dominant term is still $\Delta x_1(t - \tau_d)$. A very useful method for determining system stability is bifurcation analysis. According to the theorem proposed [27], the characteristic equation can be written as

$$P_1(\lambda) + P_2(\lambda)e^{-\lambda\tau} = 0, \tag{7}$$

where

$$\begin{aligned} P_1 &= \lambda^2 + 2\xi\omega_n\lambda + \omega_n^2, \\ P_2 &= -\omega_t^2. \end{aligned} \tag{8}$$

When the real part of a certain eigenvalue changes from negative to zero or even to positive, the time-delay increased may cause the occurrence of Hopf bifurcation. That is to say, there exists a critical time-delayτ_{dc}, at which the system with time-delay feedback control will loose stability and then the following characteristic equation has a purely imaginary root [27]. Suppose that $\lambda = i\nu$ is the purely imaginary root of the characteristic equation:

$$R_1(\nu) + iQ_1(\nu) + \left[R_2(\nu) + iQ_2(\nu)\right]\left[\cos(\nu\tau) - i\sin(\nu\tau)\right] = 0, \tag{9}$$

where

$$\begin{aligned} R_1(\nu) &= -\nu^2 + \omega_n^2, \\ R_2(\nu) &= -\omega_t^2, \\ Q_1(\nu) &= 2\xi\omega_n\nu, \\ Q_2(\nu) &= 0. \end{aligned} \tag{10}$$

Separating the real and imaginary parts of the above-mentioned equation may give

$$\begin{aligned} &R_1(\nu) + R_2(\nu)\cos(\nu\tau) + Q_2(\nu)\sin(\nu\tau) = 0, \\ &Q_1(\nu) - R_2(\nu)\sin(\nu\tau) + Q_2(\nu)\cos(\nu\tau) = 0. \end{aligned} \tag{11}$$

By squaring the above equations and then summing the results, we may obtain a quadratic equation after defining a new variable $\mu = \nu^2$:

$$\mu^2 + \left(4\xi^2 - 2\right)\omega_n^2\mu + \left(\omega_n^4 - \omega_t^4\right) = 0. \tag{12}$$

The roots of equation (12) can be obtained as

$$\mu_{1,2} = \frac{\left(2 - 4\xi^2\right)\omega_n^2 \pm \sqrt{16\xi^2\left(\xi^2 - 1\right)\omega_n^4 + 4\omega_t^4}}{2} = \left(1 - 2\xi^2\right)\omega_n^2 \pm \sqrt{\Delta}. \tag{13}$$

Due to the fact that $1 - 2\xi^2 > 0$ is always satisfied for engineering applications and if $\Delta \geq 0$ equation (12) has one positive root at least, then the critical time-delayτ_{dc} can also

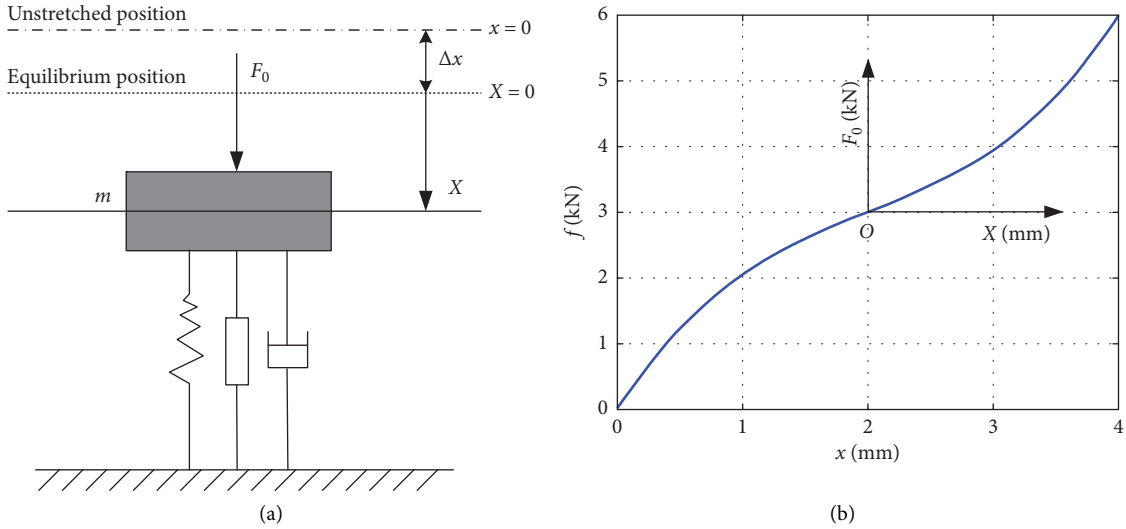

Figure 2: A single DOF nonlinear VIS: (a) system model and (b) load-displacement curve.

be acquired. So, the system goes into the state of chaos through Hopf bifurcation only when

$$K_{tc} \geq 2\xi\sqrt{\left(1-\xi^2\right)}K_1, \tag{14}$$

where ξ is the damping ratio. The relationship in equation (14) reveals that the critical control gain K_{tc} is only related to ξ and K_1 of the isolation system.

Figure 3 plots the variation of the critical control gain versus the equivalent linear stiffness for different damping ratios. Obviously, K_{tc} is linearly dependent on system stiffness K_1 and nonlinearly dependent on the damping ratio ξ. It delivers an important clue that the system can be much easily disturbed into the chaotic state when the system's stiffness and damping are small. This finding motivates us to look for small stiffness isolation system, which is beneficial not only for chaotification but also for vibration attenuation. We will show later that small control gain leads to small control energy and results in low intensity of chaotified line spectra.

The nonlinear VIFRS [14] can be regarded as a double DOF mass-spring system, as shown in Figure 4. M_1 and M_2 denote the isolated equipment and the floating raft, respectively. M_1 is supported by a linear damper and a nonlinear spring which possesses quadric and cubic nonlinearity. M_2 is supported by a linear damper and a linear spring which are connected with a fixed ground base. There

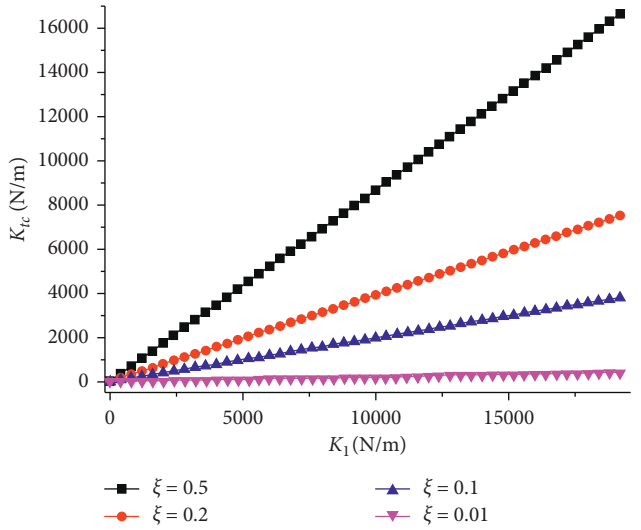

Figure 3: The critical control gain K_{tc} of a single DOF VIS with time-delay control for chaotification versus different equivalent linear stiffnesses K_1 and different damping ratios ξ.

is an actuator installed between M_1 and M_2, which is utilized to implement time-delay feedback control for chaotification.

The governing equations with time-delay feedback control are given by

$$\begin{aligned} M_1\ddot{x}_1 &= -C_1\left(\dot{x}_1-\dot{x}_2\right)-\left(K_1-2U_1H+3U_2H^2\right)\left(x_1-x_2\right)+\left(U_1-3U_2H\right)\left(x_1-x_2\right)^2-U_2\left(x_1-x_2\right)^3+F_0\cos\omega_0 t+K_t\varphi\left(\tau_d\right),\\ M_2\ddot{x}_2 &= -C_2\dot{x}_2-K_2x_2+C_1\left(\dot{x}_1-\dot{x}_2\right)+\left(K_1-2U_1H+3U_2H^2\right)\left(x_1-x_2\right)-\left(U_1-3U_2H\right)\left(x_1-x_2\right)^2+U_2\left(x_1-x_2\right)^3-K_t\varphi\left(\tau_d\right), \end{aligned} \tag{15}$$

where C_1 is the damping coefficient of the nonlinear vibration isolator; K_1, U_1, and U_2 are the linear, quadric, and cubic stiffness coefficients of the nonlinear vibration isolator, respectively. The equivalent linear stiffness at the static equilibrium point is $K_0 = K_1 - 2U_1H + 3U_2H^2$, where $H = h_1 - h_2$, C_2 is the damping coefficient of the damper between the floating raft and fixed ground, K_2 is the stiffness coefficient of the linear spring, F_0 and ω_0 are the amplitude

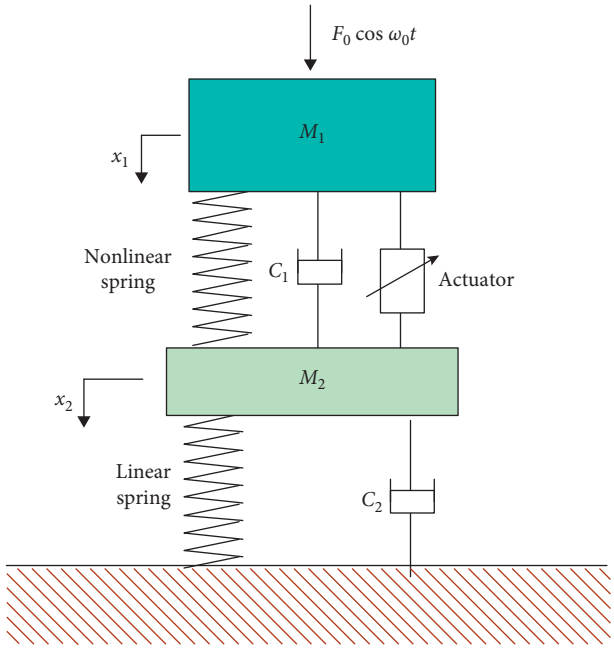

Figure 4: The structure diagram of a double DOF VIFRS.

and frequency of the harmonic excitation, respectively, K_t is the feedback control gain, and $\varphi(\tau_d)$ is the time-delay feedback control function.

For the double-layer VIS with time-delay control [14], the derivation of critical control gain is much complicated, and it can only be expressed in an implicit form. We are interested in the critical boundary for the control gain where chaotification can be implemented effectively. To find the critical condition for chaotification in the time-delay system (15), we firstly impose a linearization on the double-layer nonlinear VIFRS at an equilibrium point. Giving a perturbation to the system, it yields a set of linearized time-delay differential equations. By taking the Laplace transform, we can get the characteristic equation from which the eigenvalues are investigated for the stability switches on the parameter domain of time-delay settings and control gains.

Figure 5 illustrates the skeleton region for the stability switches on the parameter plane of the time-delay and control gain. The white region indicates the feasible area where we can apply chaotification, while the region marked in gray color denotes the infeasible area for chaotification. The critical boundaries consist of a number of solid curves. In Figure 5(a), there is a region bracketed by two dashed lines in vertical direction. As the time-delay increases to infinity $\tau \longrightarrow \infty$, these dashed lines define the boundary for chaotification. The corresponding value K_{tc} of the control gain is the required minimum control gain, regarded as the critical control gain. For the case where the system stiffness is set at $K_0 = 9600\,(\mathrm{N/m})$, as shown in Figure 5(a), the critical value of the control gain is $|K_{tc}| = 2112\,(\mathrm{N/m})$. When the system stiffness is decreased to $K_0 = 2400\,(\mathrm{N/m})$, as shown Figure 5(b), the skeleton structure is similar but the critical control gain becomes much smaller, as $|K_{tc}| = 1224\,(\mathrm{N/m})$. It reveals that when the system stiffness decreases the critical control gain decreases as well, very similar to the case of the single DOF system.

To understand the relationship between the critical control gain and the system's settings, Figure 6 shows the effects of the variation of the equivalent linear stiffness and damping on the critical control gains. With the increase of the equivalent linear stiffness K_0, the critical control gain K_{tc} increases nonlinearly unlike the linear relationship of a single DOF VIS. The curve trend also shows the significant effect for the variation of the damping coefficients C_1 and C_2 on the critical control gain. It strongly implies that small control energy required for chaotification greatly depends on small stiffness K_0 and small damping of the system. Especially, when K_0 is small, K_{tc} drops quickly with the decrease of K_0.

We know that the feedback control gain K_t represents the level of control energy to be inputted. The increase of the control gain leads to the increase of vibration amplitude generally, and accordingly the intensity of the line spectra increases as well, surely harmful to the concealment capability of underwater vehicles. In order to explain this fact quantitatively, we define the intensity of line spectra as the root mean square values of the normal difference between the spectrum peak values with control and the spectrum value at excitation frequency without control. We can obtain the relationship between the intensity of the line spectra and the feedback control gain, as shown in Figure 7.

Figure 7 plots the intensity of the line spectra under the variation of feedback control gain K_t. Obviously, the intensity of the line spectra is linearly dependent on the K_t approximately. As the absolute value of control gain increases, the intensity of line spectra increases proportionally. This diagram indicates that the smaller control leads to the lower intensity of line spectra.

3. Controller for a QZS Vibration Isolation System

In this section, the QZS system [26] is introduced to a double-layer VIS for chaotification due to its favorable feature of quasi-zero-stiffness. Based on this system, the analytical function of time-delay feedback control is derived by using the methodology [17].

In the double-layer isolation system, as shown in Figure 8, we consider a QZS system placed on the upper layer and a linear isolation system placed on the bottom layer. It is known that the QZS system [26] has the characteristics of high static and low dynamic stiffness. At the equilibrium state, the QZS system theoretically has zero stiffness, which is a perfect model for chaotification in terms of small energy control.

The QZS isolation system uses the negative stiffness of magnetic springs to offset the positive stiffness at the equilibrium state yielding the property of zero stiffness, which offers high static stability but very low dynamic stiffness around the equilibrium state. The theoretical analysis and experimental results [26] show the excellent attenuation performance in terms of the force transmissibility in comparison with conventional vibration isolation

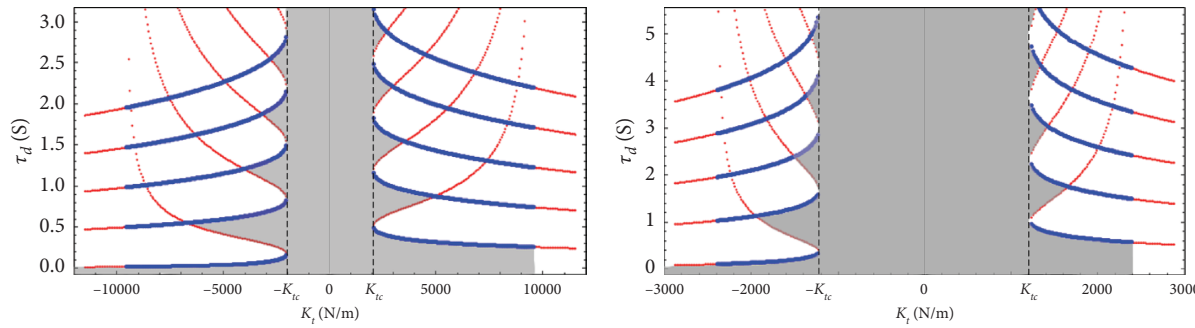

FIGURE 5: The skeleton for stability switches on the parameter plane of the time delay and control gain, indicating the feasible area (white) and infeasible area (gray) for chaotification when the system stiffness is (a) $K_0 = 9600\,(\mathrm{N/m})$ and (b) $K_0 = 2400\,(\mathrm{N/m})$.

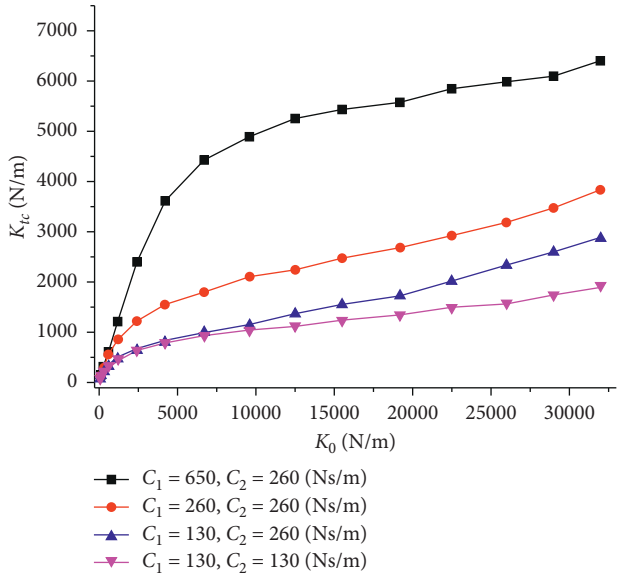

FIGURE 6: The critical control gain for chaotification versus different equivalent linear stiffnesses for different damping (C_1 and C_2 are the damping coefficients of the double-layer system, respectively).

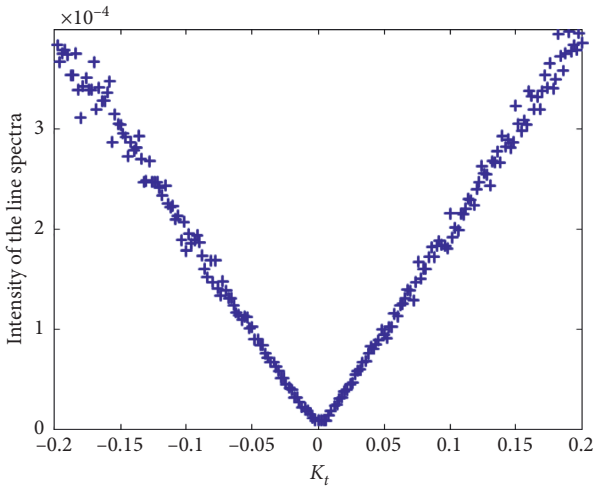

FIGURE 7: The intensity of the line spectra versus feedback control gain ($\sigma = 50, \tau = 20$).

technology. Note that this mechanical property provides a combination of two advantages. Number one, it can most effectively isolate vibration due to its inherent low natural frequency, especially outperform in the low-frequency band; number two, it allows us to use small control for chaotification.

The stiffness of the QZS system can be modeled by a unique cubic term of displacement [26], while there is no linear stiffness. The equations for the double-layer QZS system with time-delay control can be formulated as follows:

$$M_1\ddot{x}_1 = -C_1(\dot{x}_1 - \dot{x}_2) - K(x_1 - x_2)^3 + F_0\cos\omega_0 t + K_t\varphi(\tau_d),$$
$$M_2\ddot{x}_2 = -C_2\dot{x}_2 - K_2x_2 + C_1(\dot{x}_1 - \dot{x}_2) + K(x_1 - x_2)^3 - K_t\varphi(\tau_d), \quad (16)$$

where C_1 and C_2 are the damping coefficient of the QZS isolator and the bottom isolator, respectively, K and K_2 are the stiffness coefficient of the QZS isolator and linear spring,

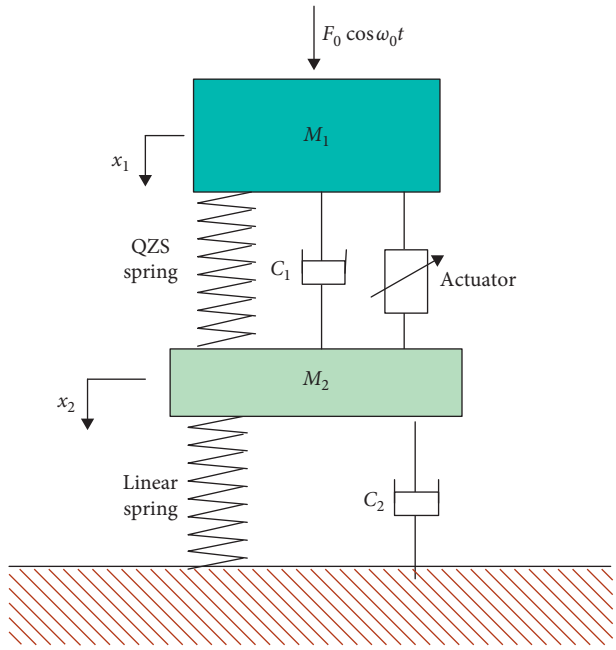

FIGURE 8: The structure diagram of a double-layer QZS system.

respectively, F_0 and ω_0 are the amplitude and frequency of the harmonic excitation, respectively, K_t is the feedback control gain, and $\varphi(\tau_d)$ is the time-delay feedback control function to be derived.

The governing equations (16) can be transformed to a standard form of the first-order governing equations, given by

$$\begin{aligned}
\dot{x}_1 &= y_1,\\
\dot{y}_1 &= -\frac{C_1}{M_1}(y_1 - y_2) - \frac{K}{M_1}(x_1 - x_2)^3 + \frac{F_0}{M_1}\cos\omega_0 t + \frac{K_t}{M_1}\varphi(\tau_d),\\
\dot{x}_2 &= y_2,\\
\dot{y}_2 &= -\frac{C_2}{M_2}y_2 - \frac{K_2}{M_2}x_2 + \frac{C_1}{M_2}(y_1 - y_2) + \frac{K}{M_2}(x_1 - x_2)^3 - \frac{K_t}{M_2}\varphi(\tau_d).
\end{aligned} \tag{17}$$

We use vector $\mathbf{x} = \begin{bmatrix} x_1 & y_1 & x_2 & y_2 \end{bmatrix}^T$ to denote the system state, where x_1 and x_2 are the displacements and y_1 and y_2 are the velocities of M_1 and M_2, respectively. The controlled system (17) can be expressed in a general form of the single-input and single-output system given by

$$\begin{aligned}
\dot{x} &= \mathbf{f}(\mathbf{x}) + \mathbf{g}(\mathbf{x})\delta\mathbf{x}(t),\\
y &= h(\mathbf{x}),
\end{aligned} \tag{18}$$

where $\delta\mathbf{x}(t) = K_t\varphi(\tau_d)$ is the input of the feedback control, $h(\mathbf{x})$ is the output function of the system, and

$$\mathbf{f}(\mathbf{x}) = \begin{bmatrix} y_1 \\ -\dfrac{C_1(y_1 - y_2)}{M_1} - \dfrac{K(x_1 - x_2)^3}{M_1} + \dfrac{F_0\cos\omega_0 t}{M_1} \\ y_2 \\ -\dfrac{C_2 y_2}{M_2} - \dfrac{K_2 x_2}{M_2} + \dfrac{C_1(y_1 - y_2)}{M_2} + \dfrac{K(x_1 - x_2)^3}{M_2} \end{bmatrix},$$

$$\mathbf{g}(\mathbf{x}) = \begin{bmatrix} 0 \\ \dfrac{1}{M_1} \\ 0 \\ -\dfrac{1}{M_2} \end{bmatrix}. \tag{19}$$

A nonlinear time-delay feedback controller for chaotification can be derived based on the differential geometry theory and the definition of Li and Yoke Chaos [19, 20]. It follows the procedure. Firstly, the above-mentioned nonlinear isolation system (18) is transformed into a standard linear system by a set of nonlinear transformation functions. The set of nonlinear transformation functions are defined by

$$\mathbf{z} = \Phi(\mathbf{x}) = \begin{bmatrix} \varphi_1(x_1, x_2, \cdots, x_n) \\ \varphi_2(x_1, x_2, \cdots, x_n) \\ \vdots \\ \varphi_n(x_1, x_2, \cdots, x_n) \end{bmatrix} = \begin{bmatrix} h(\mathbf{x}) \\ L_f h(\mathbf{x}) \\ \vdots \\ L_f^{n-1} h(\mathbf{x}) \end{bmatrix}, \tag{20}$$

where $\Phi(\mathbf{x})$ is a partial diffeomorphism and $L_f h(\mathbf{x}), \ldots, L_f^{n-1} h(\mathbf{x})$ are Lie derivatives. If the relative degree in a neighborhood of equilibrium point is exactly equal to the degree of the system, the nonlinear isolation system can be exactly transformed into a standard linear system as

$$\dot{z} = \mathbf{A}\mathbf{z} + \mathbf{B}v, \tag{21}$$

where $\mathbf{z}$ is the state vector of the linear system, v is the control function, $\mathbf{A}$ is the state coefficient matrix, and $\mathbf{B}$ is the control coefficient matrix. A nonlinear time-delay controller for chaotification in this linearized system can be derived through the technique [19, 20].

Based on the lemma below, the output function of $h(\mathbf{x})$ can be obtained and the control function of $\delta\mathbf{x}(t)$ for chaotification can be designed accordingly. The Lemma from nonlinear control theory is listed as follows.

Lemma 1. *(see [28]) A nonlinear control system is feedback linearizable on a neighborhood D of an equilibrium point if and only if*

(1) $rank\left[\, \mathbf{g}(\mathbf{x}) \;\; ad_f\mathbf{g}(\mathbf{x}) \;\; \cdots \;\; ad_f^{n-1}\mathbf{g}(\mathbf{x}) \,\right] = n, \quad x \in D$

(2) $span\left\{\mathbf{g}(\mathbf{x}), ad_{\mathbf{f}}\mathbf{g}(\mathbf{x}), \cdots, ad_{\mathbf{f}}^{n-2}\mathbf{g}(\mathbf{x})\right\}$ *is involutive on D*

Then, a solution of output $y = h(\mathbf{x})$ *from the following partial differential equations can be determined:*

$$\frac{\partial h(\mathbf{x})}{\partial \mathbf{x}}\left[\, \mathbf{g}(\mathbf{x}) \;\; ad_f\mathbf{g}(\mathbf{x}) \;\; \ldots \;\; ad_f^{n-2}\mathbf{g}(\mathbf{x}) \,\right] = 0. \tag{22}$$

Point $A(0, 0, 0, 0)$ is an equilibrium point of system (17). Based on this, we can acquire an analytical time-delay control function with Lemma 1. According to the definition, we can obtain $ad_f\mathbf{g}(\mathbf{x})$, $ad_f^2\mathbf{g}(\mathbf{x})$, and $ad_f^3\mathbf{g}(\mathbf{x})$, respectively. Using the parameter $a = x_1 - x_2$, we have

$$ad_f\mathbf{g}(\mathbf{x}) = \frac{\partial \mathbf{g}}{\partial \mathbf{x}}\mathbf{f} - \frac{\partial \mathbf{f}}{\partial \mathbf{x}}\mathbf{g} = \begin{bmatrix} -\dfrac{1}{M_1} \\ \dfrac{C_1}{M_1^2} + \dfrac{C_1}{(M_1 M_2)} \\ \dfrac{1}{M_2} \\ -\dfrac{C_1}{(M_1 M_2)} - \dfrac{C_1}{M_2^2} - \dfrac{C_2}{M_2^2} \end{bmatrix}, \tag{23}$$

$$\begin{aligned} \mathrm{ad}_{\mathbf{f}}^2\mathbf{g}(\mathbf{x}) &= \frac{\partial(\mathrm{ad}_{\mathbf{f}}\mathbf{g}(\mathbf{x}))}{\partial \mathbf{x}}\mathbf{f} - \frac{\partial \mathbf{f}}{\partial \mathbf{x}}(\mathrm{ad}_{\mathbf{f}}\mathbf{g}(\mathbf{x})) \\ &= \begin{bmatrix} -\dfrac{C_1(M_1+M_2)}{(M_1^2 M_2)} \\ \dfrac{\left[C_1C_2M_1^2 - 3a^2KM_1M_2(M_1+M_2) + C_1^2(M_1+M_2)^2\right]}{(M_1^3M_2^2)} \\ \dfrac{\left[C_2M_1 + C_1(M_1+M_2)\right]}{(M_1M_2^2)} \\ \dfrac{\left[-C_1^2(M_1+M_2)^2 - C_1C_2M_1(2M_1+M_2) + M_1(-C_2^2M_1 + M_2(K_2M_1 + 3a^2K(M_1+M_2)))\right]}{(M_1^2M_2^3)} \end{bmatrix}, \end{aligned} \tag{24}$$

$$ad_f^3\mathbf{g}(\mathbf{x}) = \frac{\partial\left(ad_f^2\mathbf{g}(\mathbf{x})\right)}{\partial \mathbf{x}}\mathbf{f} - \frac{\partial \mathbf{f}}{\partial \mathbf{x}}\left(ad_f^2\mathbf{g}(\mathbf{x})\right) = \begin{bmatrix} \Lambda_1 \\ \Lambda_2 \\ \Lambda_3 \\ \Lambda_4 \end{bmatrix}, \tag{25}$$

where

$$\begin{aligned} \Lambda_1 &= -\frac{\left[C_1C_2M_1^2 - 3a^2KM_1M_2(M_1+M_2) + C_1^2(M_1+M_2)^2\right]}{(M_1^3M_2^2)}, \\ \Lambda_2 &= \frac{\left[2C_1^2C_2M_1^2(M_1+M_2) + C_1^3(M_1+M_2)^3 + C_1M_1\left(C_2^2M_1^2 - M_2\left(K_2M_1^2 + 6a^2K(M_1+M_2)^2\right)\right) - 3aKM_1^2M_2(aC_2M_1 + 2M_2(M_1+M_2)(y_1-y_2))\right]}{(M_1^4M_2^3)}, \\ \Lambda_3 &= \frac{\left[C_1^2(M_1+M_2)^2 + C_1C_2M_1(2M_1+M_2) + M_1(C_2^2M_1 - M_2(K_2M_1 + 3a^2K(M_1+M_2)))\right]}{(M_1^2M_2^3)}, \\ \Lambda_4 &= \left[-C_1^3(M_1+M_2)^3 - C_1^2C_2M_1\left(3M_1^2 + 4M_1M_2 + M_1^2\right) + C_1M_1\left(-C_2^2M_1(3M_1+M_2) + M_2\left(6a^2K(M_1+M_2)^2 + K_2M_1(2M_1+M_2)\right)\right)\right. \\ &\quad \left. + M_1^2\left(-C_2^3M_1 + C_2M_2\left(2K_2M_1 + 3a^2K(2M_1+M_2)\right) + 6aKM_2^2(M_1+M_2)(y_1-y_2)\right)\right]/\left(M_1^3M_2^4\right). \end{aligned} \tag{26}$$

After simplification of matrix transformation and inserting the particular values of the system parameters, we can determine the rank of matrix $\left[\mathbf{g}\ \ ad_{\mathbf{f}}\mathbf{g}\ \ ad_{\mathbf{f}}^2\mathbf{g}\ \ ad_{\mathbf{f}}^3\mathbf{g}\right]$.

Next, we will determine the rank of matrix $\left[\mathbf{g}\ \ ad_{\mathbf{f}}\mathbf{g}\ \ ad_{\mathbf{f}}^2\mathbf{g}\ \ [\mathrm{ad}_{\mathbf{f}}\mathbf{g}, \mathrm{ad}_{\mathbf{f}}^2\mathbf{g}]\right]$ in order to estimate the second condition of Lemma 1:

$$\left[\mathbf{g}, ad_f^2\mathbf{g}\right] = \frac{\partial\left(ad_f^2\mathbf{g}(\mathbf{x})\right)}{\partial\mathbf{x}}\mathbf{g} - \frac{\partial\mathbf{g}}{\partial\mathbf{x}}\left(ad_f^2\mathbf{g}(\mathbf{x})\right) = \begin{bmatrix}0\\0\\0\\0\end{bmatrix}, \tag{27}$$

$$\left[\mathrm{ad}_{\mathbf{f}}\mathbf{g}, \mathrm{ad}_{\mathbf{f}}^2\mathbf{g}\right] = \frac{\partial\left(\mathrm{ad}_{\mathbf{f}}^2\mathbf{g}(\mathbf{x})\right)}{\partial\mathbf{x}}\mathrm{ad}_{\mathbf{f}}\mathbf{g} - \frac{\partial\left(\mathrm{ad}_{\mathbf{f}}\mathbf{g}\right)}{\partial\mathbf{x}}\left(\mathrm{ad}_{\mathbf{f}}^2\mathbf{g}(\mathbf{x})\right) = \begin{bmatrix}0\\\dfrac{6aK\left(M_1+M_2\right)^2}{\left(M_1^3M_2^2\right)}\\0\\-\dfrac{6aK\left(M_1+M_2\right)^2}{\left(M_1^2M_2^3\right)}\end{bmatrix}. \tag{28}$$

For system (16), we assign a set of parameters:

$$\begin{aligned} M_1 &= 85\,\mathrm{kg},\\ M_2 &= 42.5\,\mathrm{kg},\\ C_1 &= C_2 = 260\,(\mathrm{Ns/m}),\\ K &= 2.80681\times10^7\left(\mathrm{N/m^3}\right),\\ K_2 &= 3.84\times10^4\,(\mathrm{N/m}), \end{aligned} \tag{29}$$

and we can evaluate the relative degree:

$$\mathrm{rank}\left[\,\mathbf{g}\;\; ad_{\mathbf{f}}\mathbf{g}\;\; ad_{\mathbf{f}}^2\mathbf{g}\;\; ad_{\mathbf{f}}^3\mathbf{g}\,\right] = 4. \tag{30}$$

Based on equations (23)–(25) and (28) and the parameter values, we can obtain

$$\mathrm{rank}\left[\,\mathbf{g}\;\; ad_{\mathbf{f}}\mathbf{g}\;\; ad_{\mathbf{f}}^2\mathbf{g}\;\; \left[\mathrm{ad}_{\mathbf{f}}\mathbf{g}, \mathrm{ad}_{\mathbf{f}}^2\mathbf{g}\right]\,\right] = 3. \tag{31}$$

Thus, we conclude that the linear subspace $\Delta = \mathrm{span}\left\{\mathbf{g}\;\; ad_f\mathbf{g}\;\; ad_f^2\mathbf{g}\right\}$ is also involutive on a neighborhood D of the equilibrium point $A(0,0,0,0)$. The controlled system (18) has a relative degree of 4 at $A(0,0,0,0)$.

From condition (22) in Lemma 1, we can derive the output function of $y = h(\mathbf{x})$ from the partial differential equations:

$$\frac{\partial h(\mathbf{x})}{\partial\mathbf{x}}\mathbf{g}(\mathbf{x}) = \frac{1}{M_1}\frac{\partial h(\mathbf{x})}{\partial y_1} - \frac{1}{M_2}\frac{\partial h(\mathbf{x})}{\partial y_2} = 0, \tag{32}$$

$$\frac{\partial h(\mathbf{x})}{\partial\mathbf{x}}ad_{\mathbf{f}}\mathbf{g}(\mathbf{x}) = -\frac{1}{M_1}\frac{\partial h(\mathbf{x})}{\partial x_1} + \left(\frac{C_1}{M_1^2} + \frac{C_1}{M_1M_2}\right)\frac{\partial h(\mathbf{x})}{\partial y_1} + \frac{1}{M_2}\frac{\partial h(\mathbf{x})}{\partial x_2} - \left(\frac{C_1}{M_1M_2} + \frac{C_1}{M_2^2} + \frac{C_2}{M_2^2}\right)\frac{\partial h(\mathbf{x})}{\partial y_2} = 0, \tag{33}$$

$$\begin{aligned}\frac{\partial h(\mathbf{x})}{\partial\mathbf{x}}ad_{\mathbf{f}}^2\mathbf{g}(\mathbf{x}) = &-\left(\frac{C_1}{M_1^2} + \frac{C_1}{M_1M_2}\right)\frac{\partial h(\mathbf{x})}{\partial x_1} + \left(\frac{C_1\left(C_2M_1^2 + C_1\left(M_1+M_2\right)^2\right)}{M_1^3M_2^2}\right)\frac{\partial h(\mathbf{x})}{\partial y_1}\\ &+\left(\frac{C_1}{M_1M_2} + \frac{C_1}{M_2^2} + \frac{C_2}{M_2^2}\right)\frac{\partial h(\mathbf{x})}{\partial x_2} + \left(\frac{-C_1^2\left(M_1+M_2\right)^2 - C_1C_2M_1\left(2M_1+M_2\right) + M_1^2\left(-C_2^2+K_2M_2\right)}{M_1^2M_2^3}\right)\frac{\partial h(\mathbf{x})}{\partial y_2} = 0.\end{aligned} \tag{34}$$

There are multiple solutions for the set of equations (32)–(34). One of the solutions for the abovementioned equations could be derived as

$$y = h(\mathbf{x}) = -\frac{K_2M_1}{C_2M_2}x_1 - \frac{K_2M_2 - C_2^2}{C_2M_2}x_2 + \frac{M_1}{M_2}y_1 + y_2. \tag{35}$$

According to Wang et al. [19, 20], if the map associated with $\delta\mathbf{x}(t)$ is a bounded chaotic map and the time-delay is sufficiently large, then the output $y(t)$ of the system equation with time-delay (17) could be chaotic. The solution of $y = h(\mathbf{x})$ is not unique and accordingly there are multiple solutions for $\delta\mathbf{x}(t)$. We may choose various bounded functional forms. Here, the sinusoidal form of

$\delta \mathbf{x}(t) = \widetilde{K}_t \sin(\sigma y(t-\tau_d))$ is utilized for the controller, and we have

$$\delta \mathbf{x}(t) = \widetilde{K}_t \sin\left[\sigma\left(-\frac{K_2 M_1}{C_2 M_2} x_1(t-\tau_d) - \frac{K_2 M_2 - C_2^2}{C_2 M_2} x_2(t-\tau_d) + \frac{M_1}{M_2}\dot{x}_1(t-\tau_d) + \dot{x}_2(t-\tau_d)\right)\right]. \tag{36}$$

By inserting the values of the system parameters, we obtain the control function:

$$\delta \mathbf{x}(t) = \widetilde{K}_t \sin\left[\sigma\left(-295.4 x_1(t-\tau_d) - 141.6 x_2(t-\tau_d) + 2\dot{x}_1(t-\tau_d) + \dot{x}_2(t-\tau_d)\right)\right], \tag{37}$$

where the control gain $\widetilde{K}_t$, the feedback frequency σ, and the time-delay τ_d are the control parameters for the nonlinear time-delay feedback controller (37).

4. Chaotification on the QZS Vibration Isolation System

We will illustrate the benefits by proposing the 2-DOF QZS isolation system for chaotification, in comparison with the case of nonlinear isolation system used in [17]. The discussion will be focused on the three aspects including the effective reduction of critical control gain, the suppression of line spectra, and how the feature of line spectra of the system would be weakened or even be eliminated by using the approach.

4.1. Effective Reduction of Critical Control Gain. We are interested in the actual reduction of the control gain when applying chaotification on the 2-DOF QZS VIS. By setting the control parameters at $\sigma = 50$ and $\tau_d = 20$ s, we will examine the persistence of chaotification across the variation of control gain $\widetilde{K}_t$, with particular concerns on the critical control gain for the onset of chaos. We will compare the difference between the nonlinear model in [14, 17] and the QZS model proposed in this paper under the same loading conditions.

Figure 9(a) shows the global bifurcation of the nonlinear model [17], and Figure 9(b) shows the global bifurcation of the QZS model (17). Line dots in the vicinity of the origin represent periodic motions, and the cloudy dots represent the onset of chaos. From Figure 9(a), we can see that chaotification occurs when $|\widetilde{K}_t| \geq 0.452$ N. For the corresponding QZS system (17), as shown in Figure 9(b), chaotification starts when $|\widetilde{K}_t| \geq 0.008$ N and maintains across the whole parametric domain. Note that there is a significant difference in the required control gain between the two systems; the minimum control for the QZS system is only about 1.77% of that, for the nonlinear system. It indicates that the QZS system outperforms the nonlinear system [17] in terms of using small control in chaotification.

Figure 9 also indicates that the small control gain gives rise to relatively low amplitude of system responses, which means small control for chaotification can lead to low intensity of line spectra as well. Apart from the benefit of using small control, the QZS system inherently enables to attenuate vibration in low-frequency bandwidth. Thus, the utilization of the QZS system allows for the synergistic benefits of both chaotification and vibration isolation and is greatly favorable and attractive to applications.

4.2. Suppression of Line Spectra. We may benefit from the introduction of the QZS system (17) into chaotification. A comparison between the system [17] and the QZS system (17) will be carried out to indicate the performance in the reduction of the intensity of line spectra.

We show a numerical example in Figure 10, where the power spectral density (PSD) of chaotified system responses is plotted for system [17] and the QZS system (17), respectively, under the same loading conditions and the external excitation. In general, the spike line of the power spectra induced by the external excitation is covered by the continuous power spectra of chaotified responses. Thus, there is no significant spike lines protruded from the base of power spectra. The profile of the power spectra also indicates the broadband nature of system responses, implying the effectiveness of chaotification for the both systems under control.

Figure 10(a) shows that the peak value for system [17] is about −71.68 dB, while Figure 10(b) shows that the peak value for the QZS system is about −81.47 dB. Obviously, in terms of line spectrum suppression, the QZS system outperforms system [17] by about 10 dB. For the interval from 0 to 20 in the frequency domain, we can see that the QZS system is more efficient in the reduction of the intensity of line spectra. This advantage lies on two factors. Number one, the control gain required for system [17] is much larger than that of the QZS system. Small control results in low intensity of line spectra. Number two, the QZS system has better attenuation ability, especially in the low-frequency bandwidth. This nature reduces the intensity of power spectra of the response.

4.3. Reconstruction of Line Spectra. In the course of numerical analysis of line spectrum reconstruction, we can observe that chaotification on the QZS vibration isolation system constantly persists across a large range of settings for the time-delayτ_d and the feedback frequency σ. The profile of power spectra could be altered by choosing different settings of the control parameter pair (τ_d, σ). We are interested in the results where the reconstructed pattern of power spectra is smooth and broadened without line spikes protruded from the base of the power spectra when applying time-delay control. The whole purpose of chaotification is to eliminate the signature of line spectra induced by vibration excitations. In this regard, optimal design [15] of the control parameter

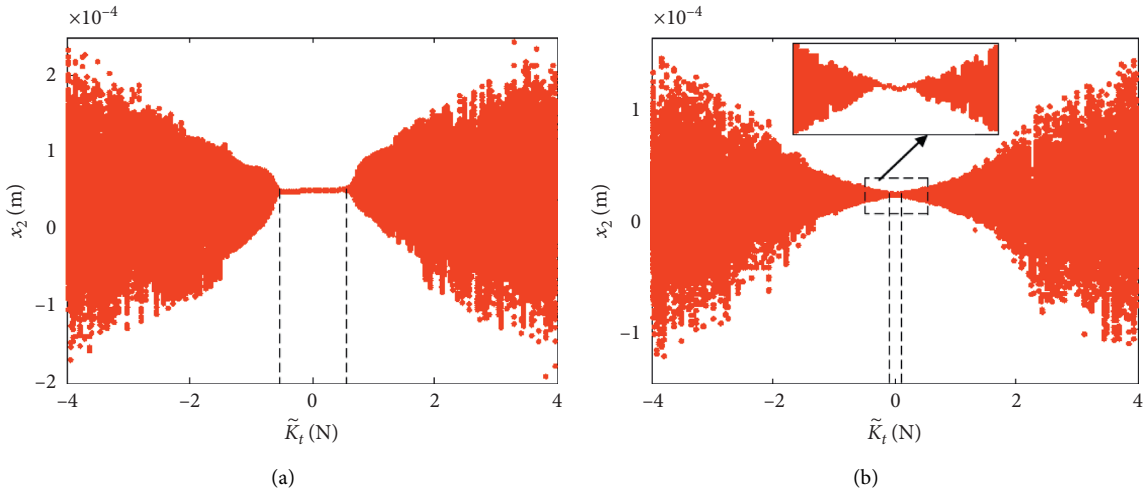

FIGURE 9: The system response versus feedback control gain $\widetilde{K}_t$; the cloudy dots represent chaotic motion and line dots denote periodic motion. (a) Response of nonlinear system [17] and (b) response of the QZS system (17).

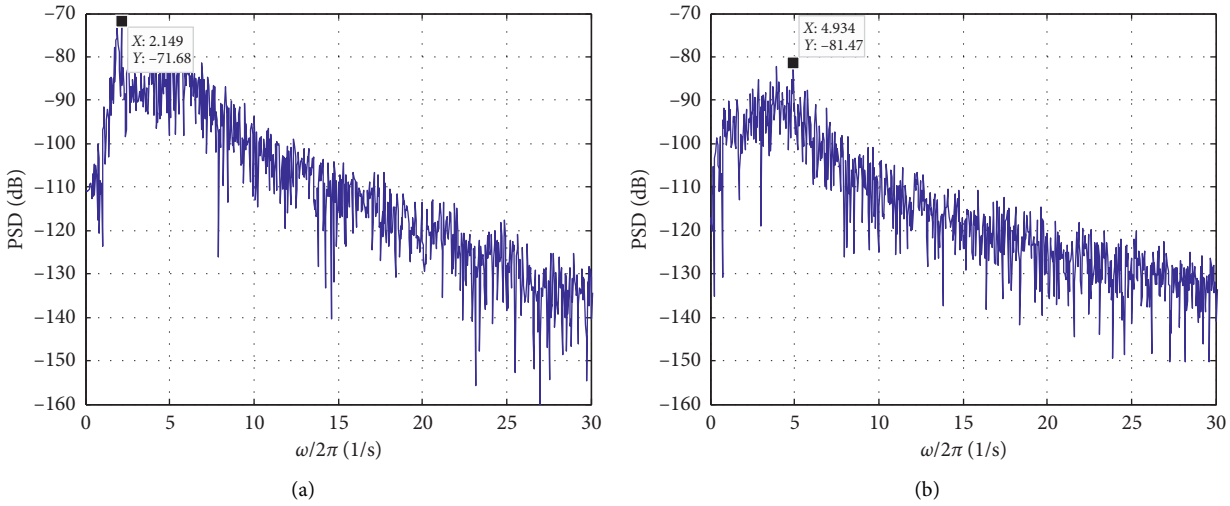

FIGURE 10: Power spectral densities of chaotified responses for (a) the nonlinear system [17] and (b) the QZS system, under the excitation at the frequency of $(\omega/2\pi) = 15.9155$.

pair (τ_d, σ) will be useful for obtaining a favorable configuration of line spectra.

In what follows, we will examine the effect of chaotification on the reconstruction of power spectra. There is a significant difference in the patterns of power spectra before and after the implementation of control. Since the formation of line spectra much depends on the excitation frequency, we consider three typical frequencies at the low frequency at 1.6711 which is smaller than the first natural frequency at 1.7311 of system (17), the intermediate frequency at 4.7746 which is in between the first and second natural frequency, and the high frequency at 22.2817 which is far away from the second natural frequency at 5.7234. We will see how the line spikes of power spectra induced by excitations, as shown in the 1st row of Figure 10, can be masked by chaotification at the three frequencies, as shown in the 2nd row of Figure 11.

Case 1. Chaotification at low-excitation frequency at $(\omega/2\pi) = 1.6711$.

Figure 11(a) illustrates the patterns of power spectra without control. There are two line spikes protruded from the base of power spectra, where the first peak represents a periodic motion at the excitation frequency and the second peak represents a subharmonic motion near the first resonance induced by the excitation. Surely, the system experiences periodic oscillations and the line feature of the power spectra is obvious. On the contrary, Figure 11(b) shows the reconstructed pattern of the power spectra after applying control, where the parameter pair of optimal control [15] is set at $(\tau_d, \sigma)_{\text{opt}} = (0.8266, 1.8026)$ and the control gain is $\widetilde{K}_{tc} = 50$ N. It can be observed that the new shape of the power spectra completely masks the second line spike but is unable to cover up the first spike. Based on extensive numerical tests, we found that it is relatively difficult to

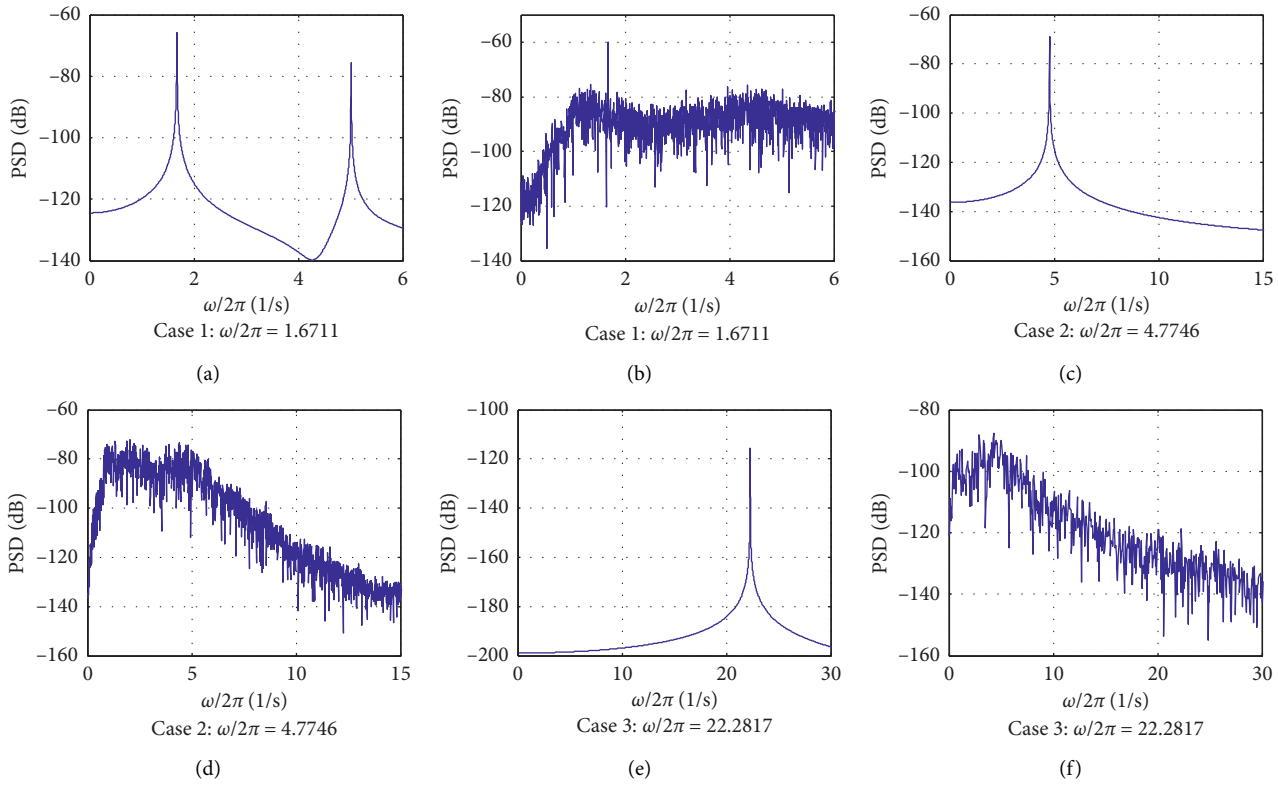

FIGURE 11: Profiles of power spectral densities of the QZS system response transmitted to the base without control (the 1st row) and with control (the 2nd row) at different excitation frequencies.

eliminate the line spikes in the low-frequency band in comparison with high-frequency band. Nevertheless, chaotification can weaken the signature of line spectra in general, and the feature of the second spike is completely eliminated.

Case 2. Chaotification at intermediate frequency at $(\omega/2\pi) = 4.7746$.

Similarly, Figure 11(c) shows the power spectra without control when applying an excitation at $(\omega/2\pi) = 4.7746$. The line spike protruded from the base indicates a periodic motion of the system at excitation frequency, and the intensity of the line spike is −68.98 dB. This line spectrum signifies the features of the machinery vibration of vehicles, for example, the operating speed according to the frequency of the line spike and the distance between the noise source and signal detector by the intensity of the line spectrum. To eliminate the features, we implement chaotification by setting the parameter pair of optimal control at $(\tau_d, \sigma)_{\text{opt}} = (0.2789, 1.1964)$, and the control gain $\widetilde{K}_{tc} = 45$ N. Figure 11(d) shows the reconstructed pattern of the power spectra of the system with the control. It is clear to be seen that the feature of the line spike is completely eliminated and replaced by the chaotic broadband spectra. Moreover, the intensity of the spectra around the excitation frequency is reduced to −79.03 dB. There is about 10 dB reduction. It means that, for certain frequency, the optimal chaotification not only covers the line spectra but also is possible to decrease its intensity.

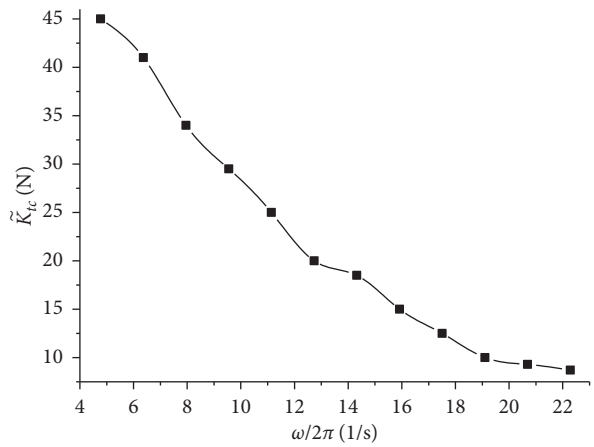

FIGURE 12: The required control gains for chaotification versus the excitation frequency.

Case 3. Chaotification at high frequency at $(\omega/2\pi) = 22.2817$.

Figure 11(e) shows the line spectrum without control when excited at $(\omega/2\pi) = 22.2817$, while Figure 11(f) shows the reformed pattern of the power spectra by applying the control at $(\tau_d, \sigma)_{\text{opt}} = (0.3970, 65.0355)$ and the control gain $\widetilde{K}_{tc} = 8.7$ N. The feature of the line spectrum at the excitation frequency is covered by the chaotic broadband spectra. However, the intensity of power spectra corresponding to the low-frequency bandwidth increases in this case.

Nevertheless, the power spectra after chaotification do not carry the information of the signal feature of the vibration source.

The required control gain for effective chaotification in general decreases as the external excitation frequency increases. This characteristic can be observed from Cases 1–3, where the control gain for chaotification reduces corresponding to the frequencies. Figure 12 plots the trend to describe the relationship between the required control gains and the excitation frequency for chaotification. In general, the higher excitation frequency, the less control energy required for chaotification. Meanwhile, the line spectra at high excitation frequency can be eliminated more easily.

5. Conclusion

The most valuable part of this paper is to propose a QZS system for chaotification that can be used to reduce the feature of line spectra induced by machinery vibration of underwater vehicles. This work combines the characteristic of small stiffness of the QZS system with the need of small control in chaotification, leading to the advantages of the reduction of the intensity of line spectra and the improvement of efficiency in the reconstruction of line spectra.

A standard procedure has been presented for the chaotification on a double-layer QZS system. We have shown the derivation of the nonlinear time-delay controller for such a system. Numerical simulations have illustrated the superior performance of the QZS system in terms of the required critical control gain and the suppression of line spectra in comparison with a nonlinear model previous studied in [17], especially outperformed in low-frequency band. In the reconstruction of line spectrum patterns, chaotification can effectively change a narrowband line spectrum induced by a harmonic excitation into a spectrum pattern with broad bandwidth. We have examined the performance of the new system in low-, intermediate-, and high-frequency bands divided according to the natural frequencies of the system. It showed that the feature of line spectra could be completely eliminated for the intermediate- and high-frequency bandwidth. It is relatively difficult to remove the line spikes in the low-frequency band, but the signal feature can be greatly weakened through a chaotification process.

Data Availability

Some or all data, models, or code that support the findings of this study are available from the corresponding author upon reasonable request.

Conflicts of Interest

The authors declare that they have no conflicts of interest.

Acknowledgments

The authors would like to appreciate Professor Daolin Xu and Chunlai Li for their help and support. This research work was supported by the National Natural Science Foundation of China (11602084), Natural Science Foundation of Hunan Province, China (2017JJ3096, 2016JJ4036), and Scientific Research Foundation of the Education Department of Hunan Province, China (17A088).

References

[1] M. W. Hiller, M. D. Bryant, and J. Umegaki, "Attenuation and transformation of vibration through active control of magnetostrictive terfenol," *Journal of Sound and Vibration*, vol. 134, no. 3, pp. 507–519, 1989.

[2] M. D. Jenkins, P. A. Nelson, R. J. Pinnington, and S. J. Elliott, "Active isolation of periodic machinery vibrations," *Journal of Sound and Vibration*, vol. 166, no. 1, pp. 117–140, 1993.

[3] C. Spelta, F. Previdi, S. M. Savaresi, G. Fraternale, and N. Gaudiano, "Control of magnetorheological dampers for vibration reduction in a washing machine," *Mechatronics*, vol. 19, no. 3, pp. 410–421, 2009.

[4] J.-J. Lou, S.-J. Zhu, L. He, and X. Yu, "Application of chaos method to line spectra reduction," *Journal of Sound and Vibration*, vol. 286, no. 3, pp. 645–652, 2005.

[5] J.-J. Lou, S.-J. Zhu, L. He, and Q.-W. He, "Experimental chaos in nonlinear vibration isolation system," *Chaos, Solitons & Fractals*, vol. 40, no. 3, pp. 1367–1375, 2009.

[6] X. Yu, S. J. Zhu, and S. Y. Liu, "A new method for line spectra reduction similar to generalized synchronization of chaos," *Journal of Sound and Vibration*, vol. 306, no. 3–5, pp. 835–848, 2007.

[7] S. Y. Liu, X. Yu, and S. J. Zhu, "Study on the chaos anti-control technology in nonlinear vibration isolation system," *Journal of Sound and Vibration*, vol. 310, no. 4-5, pp. 855–864, 2008.

[8] N. F. Rulkov, M. M. Sushchik, L. S. Tsimring, and H. D. I. Abarbanel, "Generalized synchronization of chaos in directionally coupled chaotic systems," *Physical Review E*, vol. 51, no. 2, pp. 980–994, 1995.

[9] Y. Li, D. Xu, Y. Fu, and J. Zhou, "Chaotification and optimization design of a nonlinear vibration isolation system," *Journal of Vibration and Control*, vol. 18, no. 14, pp. 2129–2139, 2012.

[10] G. L. Wen, Y. Z. Lu, Z. Y. Zhang, C. S. Ma, H. F. Yin, and Z. Cui, "Line spectra reduction and vibration isolation via modified projective synchronization for acoustic stealth of submarines," *Journal of Sound and Vibration*, vol. 324, no. 3–5, pp. 954–961, 2009.

[11] D. L. Xu, "Control of projective synchronization in chaotic systems," *Physical Review E*, vol. 63, no. 2, Article ID 027201, 2001.

[12] Z. H. Zhang, S. J. Zhu, and S. Y. Liu, "A new method of chaotic anti-control for line spectra reduction of vibration isolation system," in *Proceedings of the ASME International Design Engineering Technical Conferences and Computers and Information in Engineering Conference*, vol. 3, pp. 31–36, The American Society of Mechanical Engineers, New York, NY, USA, August 2010.

[13] J. X. Zhou, D. L. Xu, and Y. L. Li, "Chaotifing duffing-type system with large parameter range based on optimal time-delay feedback control," in *Proceedings of 2010 International Workshop on Chaos-Fractal Theories and Applications*, pp. 121–126, Kunming, China, October 2010.

[14] Y. L. Li, D. L. Xu, Y. M. Fu, and J. X. Zhou, "Stability and chaotification of vibration isolation floating raft systems with time-delayed feedback control," *Chaos: An Interdisciplinary Journal of Nonlinear Science*, vol. 21, no. 3, Article ID 033115, 2011.

[15] J. Zhou, D. Xu, J. Zhang, and C. Liu, "Spectrum optimization-based chaotification using time-delay feedback control," *Chaos, Solitons & Fractals*, vol. 45, no. 6, pp. 815–824, 2012.
[16] Y. Li, D. Xu, Y. Fu, and J. Zhou, "Nonlinear dynamic analysis of 2-DOF nonlinear vibration isolation floating raft systems with feedback control," *Chaos, Solitons & Fractals*, vol. 45, no. 9-10, pp. 1092–1099, 2012.
[17] J. Zhang, D. Xu, J. Zhou, and Y. Li, "Chaotification of vibration isolation floating raft system via nonlinear time-delay feedback control," *Chaos, Solitons & Fractals*, vol. 45, no. 9-10, pp. 1255–1265, 2012.
[18] Y. Li, D. Xu, Y. Fu, and J. Zhou, "Chaotification of a nonlinear vibration isolation system by dual time-delayed feedback control," *International Journal of Bifurcation and Chaos*, vol. 23, no. 6, Article ID 1350096, 2013.
[19] X. F. Wang, G. Chen, and X. Yu, "Anticontrol of chaos in continuous-time systems via time-delay feedback," *Chaos: An Interdisciplinary Journal of Nonlinear Science*, vol. 10, no. 4, pp. 771–779, 2000.
[20] X. F. Wang, "Generating chaos in continuous-time systems via feedback control," in *Chaos Control: Theory and Applications*, G. R. Chen and X. Yu, Eds., vol. 292, pp. 179–204, Springer, Berlin, Germany, 2003.
[21] A. Carrella, M. J. Brennan, and T. P. Waters, "Static analysis of a passive vibration isolator with quasi-zero-stiffness characteristic," *Journal of Sound and Vibration*, vol. 301, no. 3–5, pp. 678–689, 2007.
[22] I. Kovacic, M. J. Brennan, and T. P. Waters, "A study of a nonlinear vibration isolator with a quasi-zero stiffness characteristic," *Journal of Sound and Vibration*, vol. 315, no. 3, pp. 700–711, 2008.
[23] A. Carrella, M. J. Brennan, I. Kovacic, and T. P. Waters, "On the force transmissibility of a vibration isolator with quasi-zero-stiffness," *Journal of Sound and Vibration*, vol. 322, no. 4-5, pp. 707–717, 2009.
[24] J. Zhou, L. Dou, K. Wang, D. Xu, and H. Ouyang, "A nonlinear resonator with inertial amplification for very low-frequency flexural wave attenuations in beams," *Nonlinear Dynamics*, vol. 96, no. 1, pp. 647–665, 2019.
[25] K. Wang, J. Zhou, C. Cai, D. Xu, and H. Ouyang, "Mathematical modeling and analysis of a meta-plate for very low-frequency band gap," *Applied Mathematical Modelling*, vol. 73, pp. 581–597, 2019.
[26] D. Xu, Q. Yu, J. Zhou, and S. R. Bishop, "Theoretical and experimental analyses of a nonlinear magnetic vibration isolator with quasi-zero-stiffness characteristic," *Journal of Sound and Vibration*, vol. 332, no. 14, pp. 3377–3389, 2013.
[27] J. Forde and P. Nelson, "Applications of Sturm sequences to bifurcation analysis of delay differential equation models," *Journal of Mathematical Analysis and Applications*, vol. 300, no. 2, pp. 273–284, 2004.
[28] A. Isidori, *Nonlinear Control Systems*, vol. 2, Springer, Berlin, Germany, 1999.